

# Cryo-EM visualization of an exposed RGD epitope on adenovirus that escapes antibody neutralization

Phoebe L. Stewart<sup>1</sup>, Charles Y. Chiu<sup>1</sup>,  
Shuang Huang, Tom Muir<sup>2</sup>,  
Yingming Zhao<sup>2</sup>, Brian Chait<sup>2</sup>,  
Patricia Mathias and Glen R. Nemerow<sup>3</sup>

Department of Immunology, The Scripps Research Institute, La Jolla, CA, <sup>1</sup>Department of Molecular and Medical Pharmacology, Crump Institute for Biological Imaging, UCLA School of Medicine, Los Angeles, CA and <sup>2</sup>Mass Spectrometry Laboratory, Rockefeller University, New York, NY, USA

<sup>3</sup>Corresponding author

**Interaction of the adenovirus penton base protein with  $\alpha_v$  integrins promotes virus entry into host cells. The location of the integrin binding sequence Arg-Gly-Asp (RGD) on human type 2 adenovirus (Ad2) was visualized by cryo-electron microscopy (cryo-EM) and image reconstruction using a mAb (DAV-1) which recognizes a linear epitope, IRGDTFATR. The sites for DAV-1 binding corresponded to the weak density above each of the five 22 Å protrusions on the adenovirus penton base protein. Modeling of a Fab fragment crystal structure into the adenovirus–Fab cryo-EM density indicated a large amplitude of motion for the Fab and the RGD epitope. An unexpected finding was that Fab fragments, but not IgG antibody molecules, inhibited adenovirus infection. Steric hindrance from the adenovirus fiber and a few bound IgG molecules, as well as epitope mobility, most likely prevent binding of IgG antibodies to all five RGD sites on the penton base protein within the intact virus. These studies indicate that the structure of the adenovirus particle facilitates interaction with cell integrins, whilst restricting binding of potentially neutralizing antibodies.**

**Keywords:** adenovirus/cryo-electron microscopy/image reconstruction/integrins/neutralization

## Introduction

Adenovirus, a non-enveloped virus with icosahedral symmetry, is a significant cause of respiratory, gastrointestinal and ocular infections of man (Brandt *et al.*, 1969; Wadell *et al.*, 1987; Horwitz, 1990). Replication-defective forms of this pathogen have been used successfully to deliver a wide variety of foreign genes into cells (Brody and Crystal, 1994). Although the primary cellular attachment receptor has not yet been identified for adenovirus, the cell surface vitronectin-binding integrins  $\alpha_v\beta_3$  and  $\alpha_v\beta_5$  have been shown to serve as co-receptors for virus internalization (Wickham *et al.*, 1993). *In vitro* studies have demonstrated that penton base interaction with  $\alpha_v$  integrins facilitates virus internalization and infection (Bai *et al.*, 1993; Wickham *et al.*, 1993; Huang *et al.*, 1995), as well as

cell membrane permeabilization (Wickham *et al.*, 1994). *In vivo*, the expression of integrin  $\alpha_v\beta_5$  on human airway epithelial cells has been shown to promote efficient adenovirus-mediated gene delivery (Goldman and Wilson, 1995).

The cell entry pathway of adenovirus is initiated by the long protruding fiber protein attaching to the primary (unidentified) cellular receptor. Different subgroups of human adenovirus (i.e. type 2 and type 3) have different fiber receptors, as they do not block each other's binding to cells (Defer *et al.*, 1990). Binding of the penton base protein to cellular  $\alpha_v$  integrins triggers viral internalization into clathrin-coated vesicles (Svensson, 1985; Wickham *et al.*, 1993). The viral particles subsequently cause disruption of the endosomal membrane by a pH-dependent mechanism (Fitzgerald *et al.*, 1983), which is still poorly understood. The penton base (Seth *et al.*, 1984) and  $\alpha_v\beta_5$  integrin (Wickham *et al.*, 1994) have been implicated in endosome disruption. Once released into the cytoplasm, adenovirus particles are transported to the nuclear pore complex (Dales and Chardonnet, 1973) where the viral genome enters the nucleus. During the cell entry process, a stepwise dismantling of the virus structure is thought to occur with the fibers dissociating first during endocytic uptake, followed by removal of other capsid proteins, so that when the partially disassembled capsid reaches the nuclear pore complex, the viral DNA can be efficiently released (Greber *et al.*, 1993). Recent studies have also suggested that penton base interaction with cell integrins is required for reactivation of the viral protease during cell entry, which allows for proper delivery of the viral genome to the nucleus of the host cells (Greber *et al.*, 1996).

The penton base, composed of a pentamer of polypeptide III, plays a critical role in the cell entry process. Penton base binding to cell integrins can be inhibited by soluble synthetic Arg-Gly-Asp (RGD) peptides, as well as by monoclonal antibodies to the functional domain of the integrin (Wickham *et al.*, 1993). The RGD sequence is conserved within a highly variable region in the penton base protein of four distinct adenovirus serotypes (representing subgroups A, B, C and E) and many adenovirus types use this sequence for infection (Neumann *et al.*, 1988; Mathias *et al.*, 1994). The penton base is the component of the adenovirus capsid that becomes most hydrophobic at pH 5.0 and, hence, is presumed to interact with the endosomal membrane (Seth *et al.*, 1985). While the penton base may bind either  $\alpha_v\beta_3$  or  $\alpha_v\beta_5$  integrin to trigger viral internalization, only  $\alpha_v\beta_5$  was found to enhance membrane permeabilization (Wickham *et al.*, 1994).

Previous cryo-electron microscopy (cryo-EM) studies combined with the X-ray crystal structure of the major capsid protein, hexon, have revealed the three-dimensional

structure of type 2 adenovirus (Ad2) at 35 Å resolution (Stewart *et al.*, 1991; Athappilly *et al.*, 1994). Each of the 12 vertices of the virus particle contains a penton complex comprising a penton base protein which is non-covalently associated with a fiber protein. Mathematical deconvolution of the cryo-EM reconstruction significantly improved the resolution and revealed the presence of 22 Å protrusions on the outer surface of the penton base (Stewart *et al.*, 1993). We predicted that these protrusions contain the RGD sequences as they represent the most accessible portion of the penton base and the RGD stretch is located within a hydrophilic region of the penton base.

This paper presents the neutralization properties and epitope specificity of a penton base mAb. Cryo-EM and image reconstruction have enabled visualization of the adenovirus–Fab complex and localized the RGD binding site on the virus surface. Modeling with crystallographic coordinates of a Fab fragment indicated the amplitude of motion of the RGD epitope. These studies reveal a novel mechanism for evasion of antibody-mediated neutralization.

## Results

### Characterization of the DAV-1 anti-penton base mAb

The antigenic specificity of the intact DAV-1 mAb was determined in an ELISA and Western blot. The DAV-1 mAb reacted with several different human adenovirus serotypes, including Ad2, Ad3 and Ad4; however, it showed only low level reactivity with an unrelated (control) virus, Epstein–Barr virus (EBV) (Figure 1A). Each of these adenovirus types contains a penton base RGD sequence and similar, but not identical, flanking sequences (Mathias *et al.*, 1994). The DAV-1 mAb also reacted with purified recombinant penton base in a Western blot, but it did not recognize different cell matrix proteins, including vitronectin, fibronectin and fibrinogen, all of which contain an integrin-binding (RGD) sequence but with very different flanking residues (Figure 1B). To test further whether the DAV-1 mAb recognizes the integrin binding (RGD) sequence in the penton base protein, we examined whether penton base binding to cells could be inhibited by the DAV-1 mAb. Incubation of the penton base protein with the DAV-1 mAb or with Fab fragments from this mAb blocked penton base binding to A549 cells (Figure 2A), consistent with the notion that this mAb recognizes the integrin binding site on the penton base protein.

Next, we determined whether the DAV-1 mAb was capable of inhibiting adenovirus infection, since the interaction of the adenovirus penton base protein with  $\alpha_V$  integrins plays an important role in viral cell entry (Bai *et al.*, 1993, 1994; Wickham *et al.*, 1993; Huang *et al.*, 1995). Preincubation of Ad2 with Fab fragments of the DAV-1 mAb inhibited infection of A549 cells, while treatment of the virus with 3-fold higher amounts of intact IgG molecules failed to inhibit adenovirus infection (Figure 2B). Further studies were performed to obtain precise measurements of DAV-1 mAb binding to the penton base by surface plasmon resonance (SPR). We observed that, at saturation, five molecules of DAV-1 Fab fragment bind to each penton base protein while, on average, only 2.8 molecules of IgG antibody can bind to

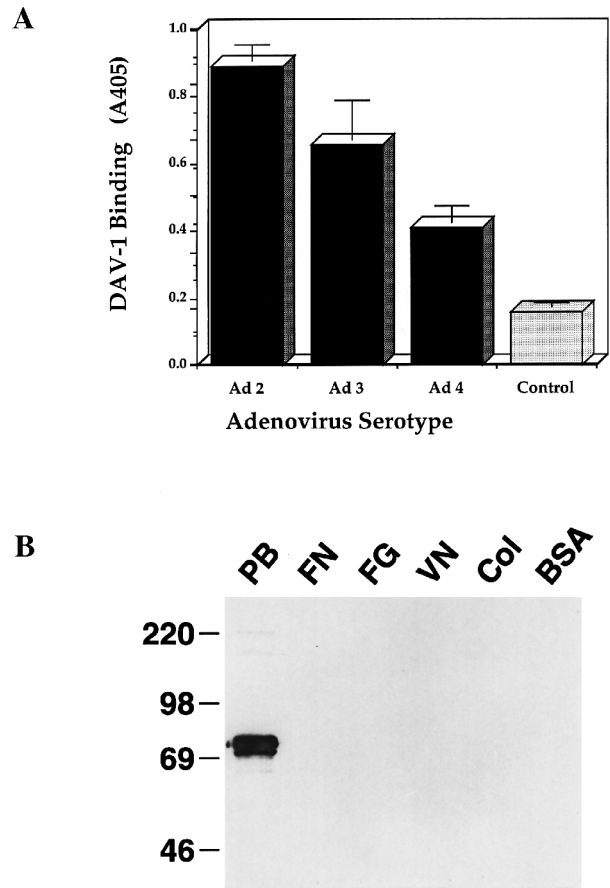


**Fig. 1.** Reactivity of the DAV-1 mAb with human adenoviruses and cell matrix proteins. **(A)** Binding of the DAV-1 mAb to different adenovirus serotypes (Ad2, Ad3 and Ad4) or to a control virus (EBV) was measured in an ELISA. **(B)** Binding of the DAV-1 mAb to the penton base (PB) or cell matrix proteins, including fibronectin (FN), fibrinogen (FG), vitronectin (VN), collagen type 1 (Col) or BSA was assessed in a Western blot.

this protein. The IgG form of the DAV-1 antibody was found to have a somewhat higher affinity for the penton base than Fab fragments ( $K_D = 1.8 \times 10^{-8}$  M and  $8.5 \times 10^{-8}$  M, respectively). Therefore, differences in affinity for the penton base protein do not account for the ability of Fab fragments to selectively mediate virus neutralization.

### Epitope mapping of the DAV-1 mAb

The DAV-1 binding site on the Ad2 penton base was rapidly identified using the recently described affinity-directed mass spectrometry approach (Zhao and Chait, 1994; Zhao *et al.*, 1996). For these studies, we arbitrarily selected a short region of the penton base, residues <sup>480</sup>MNDHAIRGDTFATRA<sup>494</sup>, that spanned the RGD motif. As a first step, two nested peptide ladders, an N-terminal set and a C-terminal set, were manually synthesized using previously described solid-phase protocols (Zhao *et al.*, 1996), such that each peptide ladder covered the entire sequence of interest and each peptide within the nested set differed by one amino acid. Each peptide ladder was then affinity-selected using the immobilized DAV-1 mAb. Those sequences which contained the complete binding epitope were thus resolved from those sequences which did not. The identities of the affinity-

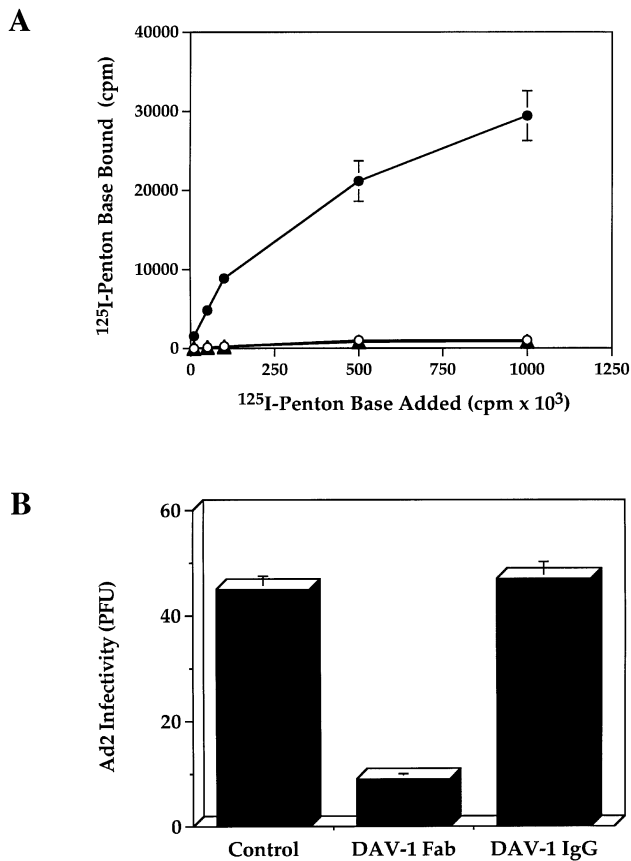


**Fig. 2.** Functional properties of the DAV-1 mAb. **(A)** Binding of [ $^{125}\text{I}$ ]penton base to A549 cells was measured in the presence of 10  $\mu\text{g}/\text{ml}$  DAV-1 mAb (IgG, open circles) or Fab fragments (closed triangles) or a control mAb (LM142, closed circles). **(B)** Ad2 infection of A549 was measured in the presence of 18  $\mu\text{g}/\text{ml}$  intact DAV-1 mAb or 3  $\mu\text{g}/\text{ml}$  Fab fragments or a control mAb by plaque assays.

selected sequences were then determined in a single step using matrix-assisted laser desorption mass spectrometry as described (Zhao and Chait, 1994; Zhao *et al.*, 1996). By simply comparing the matrix-assisted laser desorption ionization (MALDI) mass spectra of the N- and C-terminal peptide ladders before and after the affinity-selection step, the exact boundaries of the linear binding sequence were identified (Figure 3). The shortest N-terminal series peptide recognized by the DAV-1 mAb contains an isoleucine (I) residue while the shortest C-terminal series peptide recognized by DAV-1 contains an arginine (R) residue. Together, these data indicated that the minimal epitope is IRGDTFATR. This result was consistent with the neutralization properties of the DAV-1 mAb and with its inability to recognize mutated recombinant penton base proteins which lack the RGD sequence (data not shown).

#### Cryo-EM structure of the adenovirus–Fab complex

Digital cryo-images of Ad2 particles complexed with DAV-1 Fab fragments were collected on a Philips CM120 with a Gatan slow-scan CCD camera (Figure 4A). The particles were observed to be randomly oriented within the thin layer of vitreous ice. It is difficult to visualize the bound Fab fragments in the raw cryo-images, as binding at all sites results in only a 2% increase in the total mass of the particle. Nevertheless, in favorable particle

orientations (Figure 4B), DAV-1 Fab density can be seen at the base of the adenovirus fiber in close proximity to the penton base protein. Digital cryo-images were also collected of uncomplexed adenovirus under identical conditions.

Selection and refinement of 48 individual particle images yielded a 19  $\text{\AA}$  resolution three-dimensional reconstruction of the adenovirus–Fab complex (Figure 5). The resolution of the reconstruction, verified by Fourier ring correlation methods, is sufficient to note detail on the hexon proteins that was not seen in the previously published structure of the mature virus particle (Stewart *et al.*, 1991, 1993). The structural features of the hexons in the reconstruction agree with the crystallographic structure of hexon (Athappilly *et al.*, 1994) and served as a suitable control for evaluating the correctness of the three-dimensional map. In addition, the crystallographic coordinates filtered to 19  $\text{\AA}$  provided a way to confirm the resolution of the reconstruction. Only short portions of the 12 protruding fibers, which are characteristic of adenovirus, are visible as the fiber is not perfectly straight and is thus mostly averaged away by the imposed icosahedral symmetry (Stewart *et al.*, 1991). Deconvolution of the map to correct for the distortions caused by the contrast transfer function (CTF) of the electron microscope was carried out as described previously (Stewart *et al.*, 1993).

A reconstruction of uncomplexed adenovirus was also calculated from 48 particle images at the same resolution (19  $\text{\AA}$ ) as the virus–Fab complex. There were no discernible differences between the two reconstructions apart from the additional Fab density above the penton base proteins. Close inspection of the uncomplexed adenovirus reconstruction showed strong protrusion density extending 22  $\text{\AA}$  above the penton base protein, as well as weaker density extending out another 24  $\text{\AA}$  (Figure 6). The weaker portion of the protrusion is only observed when the penton base is contoured at just above the noise level, and it suggests the presence of a mobile surface loop of the penton base protein.

Difference imaging between the virus–Fab structure and the uncomplexed structure allowed the Fab density to be separated from the adenovirus capsid density. The isolated Fab density is observed as a continuous ring above each penton base with connections to the penton base protrusions (Figure 7A and B). To visualize the diffuse Fab density, the isosurface threshold had to be lowered to just above the noise level. The presence of the weak Fab density was confirmed by calculating an independent reconstruction from an additional 48 adenovirus–Fab particle images. The weak Fab density extends 70  $\text{\AA}$  above the penton base protrusions, roughly the expected height for a Fab fragment, and 92  $\text{\AA}$  radially outwards from the fiber protein. The total integrated Fab density is 86% of that expected for five rigidly bound Fab fragments, and as the edge of Fab density is not well defined, our integrated density is probably an underestimate. In addition, the Fab volume is roughly twice that expected, supporting our hypothesis of a mobile surface epitope on the penton base protein.

Since the Fab density is observed to connect only to the mobile portion of the penton base protrusion, we conclude that the DAV-1 epitope (IRGDTFATR) is located within this density. In Figure 6D we show a stylized,

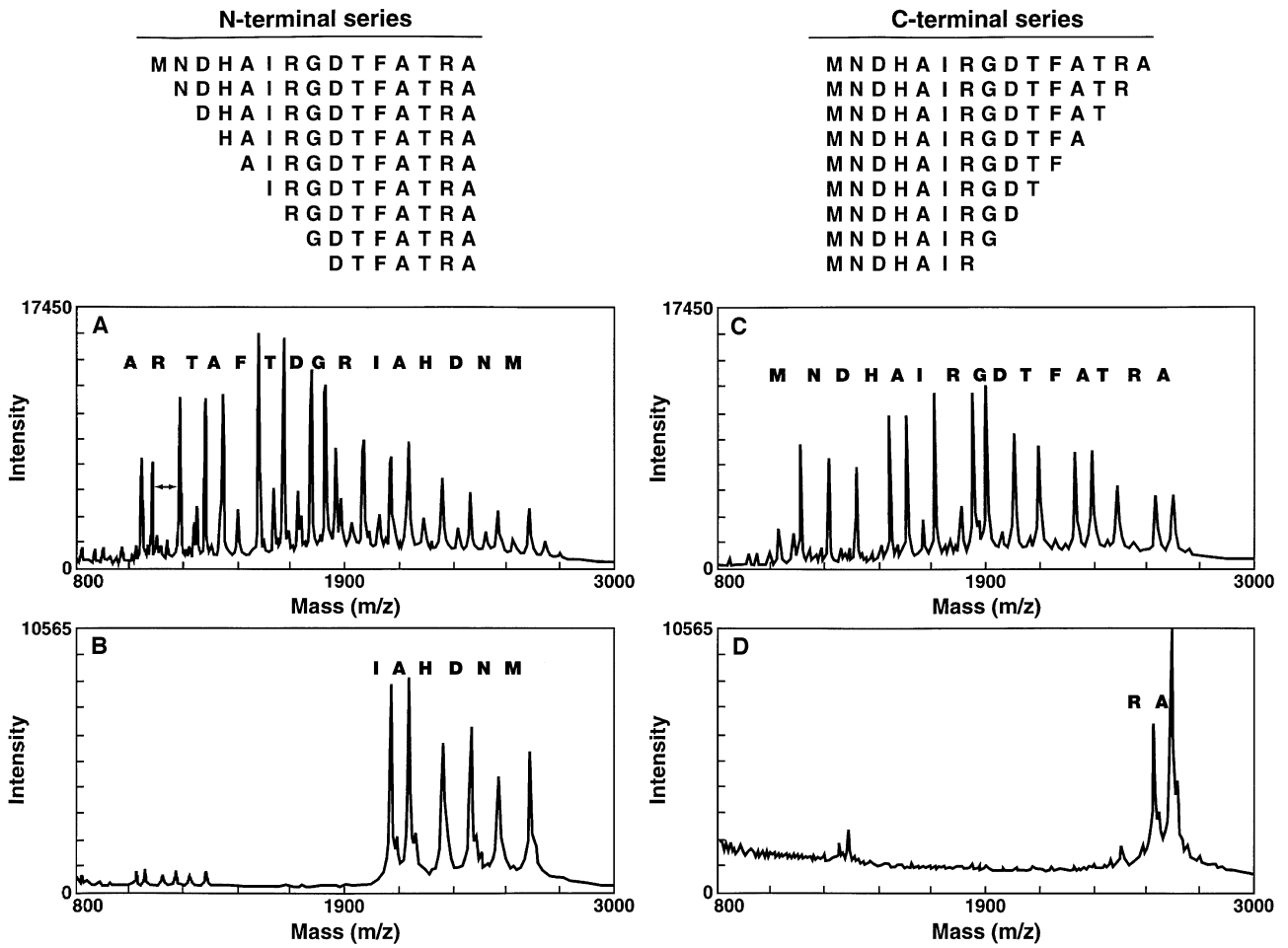


**Fig. 3.** Epitope mapping of the DAV-1 mAb by affinity-directed mass spectrometry. A series of N-terminal (left) or C-terminal peptides (right) was analyzed by matrix-assisted mass spectrometry before (A and C) or after affinity-selection (B and D) with the DAV-1 mAb. A comparison of the MALDI mass spectra of the N- and C-terminal peptide ladders, before and after the affinity-selection step, allowed identification of the exact boundaries of the linear peptide sequence (IRGDTFATR) recognized by the DAV-1 mAb.

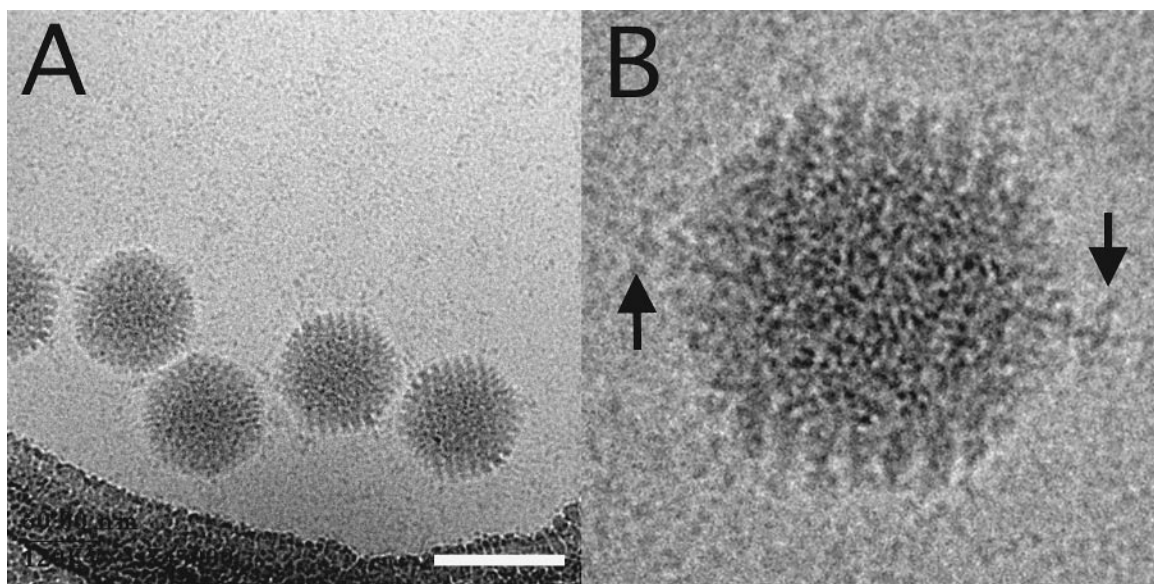


**Fig. 4.** Digital cryo-electron micrographs of adenovirus–DAV-1 complexes. (A) A representative field of particles with a 1000 Å scale bar. (B) An enlargement of one particle with arrows indicating regions of density attributed to DAV-1 Fab fragments.

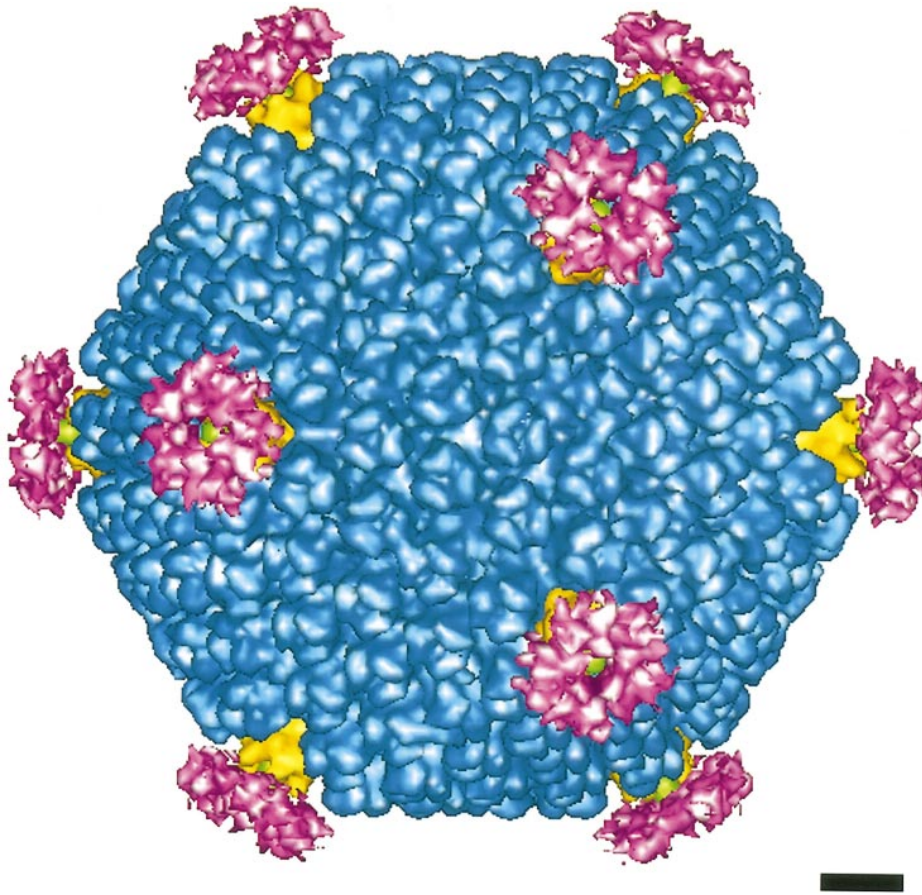


**Fig. 5.** A cryo-EM image reconstruction of the adenovirus–DAV-1 Fab complex. The penton base capsomers at the icosahedral vertices are shown in yellow, the reconstructed portion of the flexible fibers in green, the remaining capsid density in blue and the Fab density in magenta. The complex is viewed along an icosahedral 3-fold axis. The scale bar is 100 Å.

mobile RGD peptide loop within the weak portion of the protrusion. Interestingly, the previously reported cryo-EM volume for the penton base was only 93% of that predicted from the molecular mass and comparison with the crystallographic hexon (Stewart *et al.*, 1993). The mobile portion of the penton base protrusion, which had not been observed previously, may account for most of the missing volume. Our volume measurements indicate ~30 amino acid residues in the top, mobile portion (Figure 6, shown in red) and an additional 60 residues in the rest of a single protrusion.

#### **Modeling of Fab binding to the penton base**

The Fab density was analyzed by mapping in crystallographic coordinates of a Fab fragment from a mAb directed against the RGD integrin-binding loop of foot-and-mouth disease virus (FMDV) (Verdaguer *et al.*, 1995). We positioned a single crystallographic Fab fragment above each penton base binding site and calculated a 19 Å resolution density map from these coordinates (Figure 7C and D). The resulting model density clearly does not match the observed cryo-EM Fab density with the model volume only accounting for 45% of the observed volume. This observation, coupled with the fact that the Fab density values are on average much lower than those of the

viral capsid, suggests that the Fab molecules are mobile, producing a diffuse reconstructed density.

The volume of the cryo-EM Fab density is large enough to map in eight distinct orientations of the Fab coordinates per binding site. The tilt angles of the modeled Fab coordinates were calculated and found to vary from 27° to 88° with respect to the fiber axis, indicating a large amplitude of motion. A 19 Å resolution density map was calculated from all of the modeled coordinates, and is depicted in Figure 7E and F as a wire mesh along with Fab fragments in five different orientations. Note that the overall shape of the wire mesh matches the shape of the observed cryo-EM Fab density (Figure 7A and B), with dimensions that agree to within 10%. The Fab coordinates used for modeling were from a crystallographic structure of a complex with a 15 residue RGD-containing peptide of the FMDV (Verdaguer *et al.*, 1995). Positioning of the RGD peptide coordinates, within the weak density at the top of the penton base protrusions, resulted in the antigenic binding sites of the Fab fragments capping the weak protrusion density (Figure 7D). As the spatial relationship between the Fab antigen binding site and the RGD peptide antigen is fixed, the observed Fab density could not have been modeled without assuming a variable location for the RGD domain. Thus, we have localized the dynamic

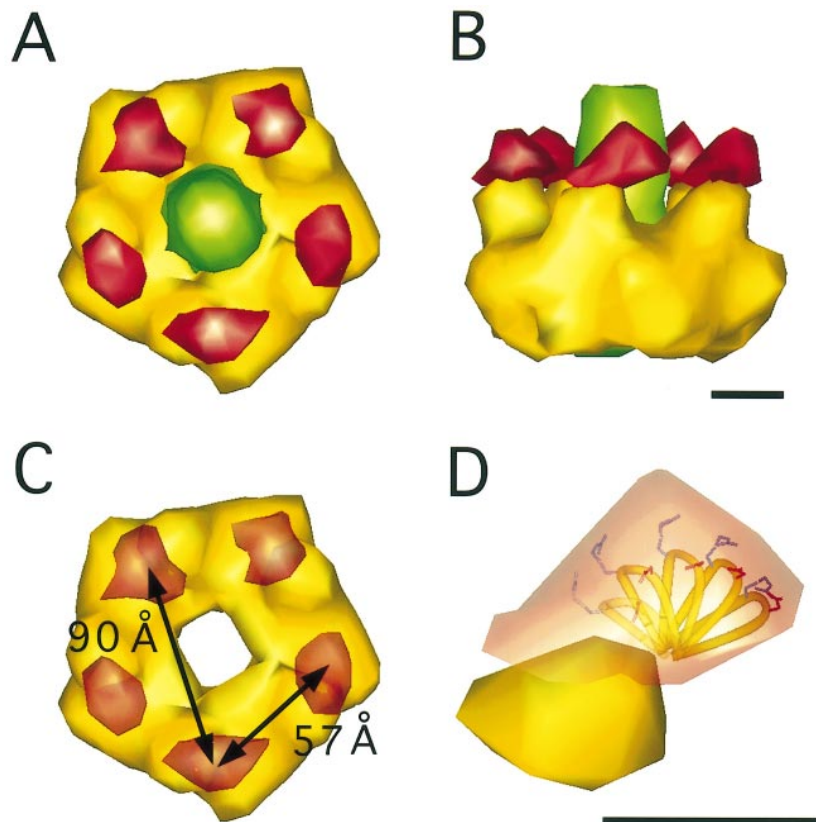


**Fig. 6.** The adenovirus penton base protrusions. (A) Top view of the penton base (yellow) and fiber (green) along with weak protrusion density (red). (B) Side view of the external portion of the penton base with fiber. (C) Top view of the penton base showing the distances between weak protrusions. (D) An enlargement of a single penton base protrusion with a loop modeled from the crystallographic FMDV RGD peptide. The arginine side chain is shown in blue, and the aspartic acid side chain in red. The loops are shaded with a transparency gradient to denote motion. The scale bars are 25 Å.

RGD epitope to within the weak density at the top of the penton base protrusion.

## Discussion

### **Neutralization properties of the DAV-1 mAb**

The identification of an adenovirus mAb that reacts specifically with an RGD epitope in the penton base protein provided an opportunity to characterize the  $\alpha_v$  integrin binding site. An unanticipated finding was that Fab fragments of the DAV-1 mAb but not IgG molecules blocked Ad2 infection (Figure 2). This represents a rare example of virus neutralization by Fab fragments rather than by IgG antibody molecules. The average center-to-center distance between the RGD epitopes on the penton base is 57 Å between adjacent protrusions (Figure 6C), similar to the minimum distance previously noted for epitope bridging by an IgG molecule (Hewat and Blaas, 1996). Therefore, bivalent binding of the DAV-1 mAb should be possible, especially since there is flexibility in both the epitope and the antibody hinge region. Our saturation binding measurement of 2.8 IgG molecules per soluble penton base protein can be explained by two bivalently and one monovalently bound antibody molecules. However, in the intact virus particle, the central fiber is an additional source of steric hindrance and apparently prevents binding of IgG molecules to all five

sites. Any unbound sites may still bind integrin because the virus is already tethered to the cell surface by the fiber protein, and this proximity may facilitate the viral interaction with integrin. In contrast, the less bulky DAV-1 Fab fragments can effectively block Ad2 infection since they are capable of binding to all of the exposed epitopes.

### **Cryo-EM reveals a mobile RGD epitope on adenovirus**

The cryo-EM structure of the Ad2–DAV-1 complex shows that the Fab fragments bind to the top of five protrusions on the penton base. The nine amino acid epitope recognized by the DAV-1 mAb was found to include the RGD motif required for  $\alpha_v$  integrin binding (Wickham *et al.*, 1993). The structure indicates a large amplitude of motion for the RGD peptide as averaged and diffuse density is observed for the Fab fragments. In contrast, cryo-EM reconstructions of other virus–Fab complexes (Smith *et al.*, 1993, 1995; Porta *et al.*, 1994) have shown strong, well-defined Fab density. In favorable cases, it has even been possible to distinguish the Fab elbow angle to within 20° from the shape of the cryo-EM density (Liu *et al.*, 1994). Our finding of a mobile epitope is consistent with two-dimensional NMR studies which showed no identifiable secondary structure for a 50 residue synthetic peptide corresponding to the Ad2 penton base RGD domain

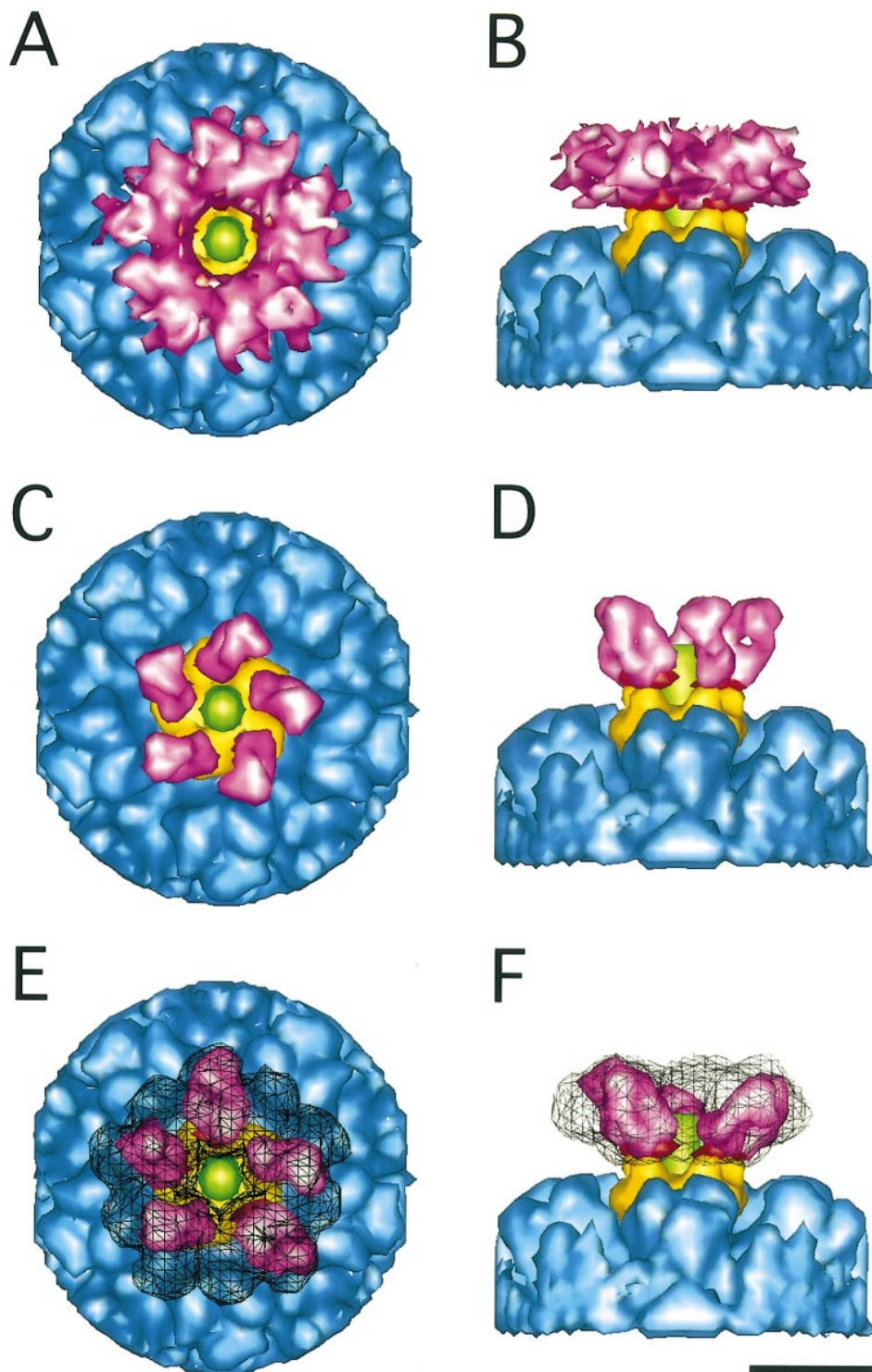


**Fig. 7.** Vertex region of adenovirus. (A and B) Top and side views of the reconstructed Ad2–DAV-1 complex. The DAV-1 Fab density has been isolated by difference imaging. (C and D) Views with a crystallographic Fab fragment, filtered to 19 Å resolution, modeled at each of the five binding sites on the penton base. (E and F) Views showing the total model density (wire mesh) obtained from Fab fragments in eight distinct orientations along with one Fab fragment bound to each site. Each Fab fragment is shown in a different orientation to suggest mobility. The color scheme is the same as in Figures 5 and 6. The scale bar is 100 Å.

(W.Chazin, personal communication). Alignment of four different adenovirus penton base proteins shows the RGD residues to be in the middle of a highly variable stretch (Mathias *et al.*, 1994). The length of the variable region

ranges from 22 residues for type 12 to 80 residues for type 2. It will be of interest to determine whether the RGD domains of other adenovirus serotypes have smaller protrusions than Ad2 and, therefore, less flexible surface

epitopes and whether this feature influences antibody neutralization and interactions with cell integrins.

Support for our finding of a mobile integrin binding site comes from NMR structures of fibronectin (Main *et al.*, 1992) and two snake venom proteins, echistatin (Atkinson *et al.*, 1994) and kistrin (Adler *et al.*, 1991), as well as the crystal structure of FMDV which all showed mobile RGD loops. Crystallographic structures of two serotypes of the picornavirus FMDV (Acharya *et al.*, 1989; Lea *et al.*, 1994), as well as two variants (Parry *et al.*, 1990) reveal that the RGD integrin binding site is at the apex of a highly mobile surface loop (~20 residues long). The finding of a mobile RGD loop in both adenovirus and FMDV, which are otherwise structurally distinct, suggests that the conformational mobility of the RGD loop may facilitate interaction with cell integrins, thus potentiating cell entry events.

### **Relationship of receptor binding sites and antibody-mediated neutralization**

Recent structure studies have revealed that the receptor binding sites on different viruses are generally accessible to neutralizing antibodies. For example, antibodies directed to the receptor binding site on human rhinovirus 14 are able to penetrate deep within the receptor binding canyon (Smith *et al.*, 1996). Both FMDV and adenovirus have exposed RGD receptor sites that are also accessible to Fab fragments of neutralizing antibodies. The adenovirus RGD site binds to both  $\alpha_v\beta_3$  and  $\alpha_v\beta_5$  integrins, and recently it has been shown that  $\alpha_v\beta_3$  integrin can function as a receptor for FMDV (Berinstein *et al.*, 1995). The mobile RGD sites on FMDV are clustered about the icosahedral 5-fold axis with roughly the same spacing as we have shown for adenovirus, but without the central fiber protein. Neutralizing monoclonal antibodies have been raised to the FMDV RGD sites, which suggests that the fiber plays an important role in allowing adenovirus to escape neutralization at its exposed RGD sites. FMDV variants escape antibody neutralization by undergoing mutations in the coat protein distal to the RGD sequence, an event that perturbs antibody binding to the integrin binding site (Parry *et al.*, 1990).

Our structural and functional studies show that adenovirus escapes neutralization by IgG antibodies directed against the RGD integrin receptor site. This is most likely achieved by the steric hindrance of the fiber and the bulky IgG molecules that are bound to a mobile epitope, which effectively shield a few RGD sites from IgG binding while still allowing interactions with cell surface integrins. Thus, the studies reported here characterize a receptor binding site that enables adenovirus to evade antibody-mediated neutralization.

## **Materials and methods**

### **Cell lines, virus and recombinant proteins**

A549, HeLa, H2981 and SW480 cell lines, adenovirus serotypes Ad2, Ad3 and Ad4 were purchased from the American Type Tissue Culture Collection (Rockville, MD). For virus isolation, HeLa cells were infected with either Ad2, Ad3 or Ad4 at a multiplicity of 10 p.f.u./cell and then harvested 48–72 h later. Cells were frozen and thawed five times to release intracellular virus particles. After removing the cell debris by high-speed centrifugation, virions were isolated by banding on a 15–40% cesium chloride gradient in 10 mM Tris-HCl, 150 mM NaCl

pH 8.1 (TBS) as reported previously (Everitt *et al.*, 1977). Banded virions were removed and then dialyzed into TBS buffer containing 10% glycerol, except for cryo-EM studies in which case the CsCl<sub>2</sub> was removed by multiple centrifugation steps in a Microcon 100 (Amicon) filtration device using pH 8.1 phosphate buffer. Recombinant Ad2 penton base containing 571 amino acids (Neumann *et al.*, 1988) was produced in Sf9 insect cells using baculovirus as previously described (Nemerow *et al.*, 1993; Wickham *et al.*, 1993).

### **Generation and characterization of the DAV-1 anti-penton base mAb**

A hybridoma (designated DAV-1) secreting a mAb of the subtype  $\gamma_1\kappa$  was generated by standard techniques. The DAV-1 mAb was purified from ascites fluids using protein G-Sepharose (HiTrap GII, Pharmacia). Fab fragments of the DAV-1 mAb were generated by papain digestion. Briefly, 1–5 mg/ml of purified DAV-1 IgG in 50 mM Tris-HCl pH 8.0, 10 mM L-cysteine, 3 mM EDTA was incubated for 7 h at 37°C in the presence of 8% w/w soluble papain (Sigma Chemical Co., St Louis, MO). The reaction was stopped by the addition of 30 mM iodoacetamide, and the Fab antibody fragments were then isolated on a Resource S FPLC column (Pharmacia) equilibrated with 50 mM MES pH 5.0. The purified Fab fragments were analyzed by SDS-PAGE and then concentrated to 2.2 mg/ml using a Centricon 10 membrane ultrafiltration device (Amicon).

Reactivity of the DAV-1 mAb with different adenovirus serotypes was quantified in an ELISA. Ninety-six well polystyrene plates (Immobilon, Dynatech) were coated with 1  $\mu$ g of penton base or with 5  $\mu$ g of purified Ad2, Ad3 or Ad4 in PBS for 18 h at 4°C. After blocking non-specific binding sites with 2% non-fat dried milk, 10  $\mu$ g/ml of purified DAV-1 mAb or an irrelevant control antibody were added to the wells for 60 min at 22°C. Antibody binding was detected by the addition of alkaline phosphatase linked to goat anti-mouse IgG followed by substrate (Sigma Chemical Co., St Louis, MO). Substrate development was quantified at 405 nm in an ELISA plate reader (Titertek, Flow laboratories). To examine whether the DAV-1 mAb also recognized RGD-containing cell matrix proteins, 1–2  $\mu$ g of recombinant penton base protein, or fibronectin, vitronectin, collagen (type 1) and fibrinogen were reacted with the DAV-1 mAb in a Western blot. Recombinant penton base or cell matrix proteins were electrophoresed on a 8–15% gradient SDS gel (Novex, San Diego, CA) and then transferred to a nitrocellulose filter (Immobilon P, Millipore). Following blocking of non-specific binding sites with 1% non-fat dried milk (Blotto), the filters were reacted with 10  $\mu$ g/ml of the DAV-1 mAb followed by incubation with alkaline phosphatase linked to goat anti-mouse IgG (Tropix, Bedford, MA) and then with a chemiluminescent substrate (CDP).

### **Functional analysis of the DAV-1 mAb**

The effect of the DAV-1 mAb on penton base binding to cell surface  $\alpha_v$  integrins was examined as follows. To  $1 \times 10^6$  A549 epithelial cells were added 10  $\mu$ g/ml of purified DAV-1 IgG or Fab fragments of the DAV-1 mAb. Varying amounts of <sup>125</sup>I-labeled penton base (10  $\mu$ Ci/ $\mu$ g) were then added to the cells in the presence or absence of a 50-fold excess of unlabeled penton base and incubated for 60 min at 4°C. Unbound penton base was removed by centrifuging the cell samples through a cushion of 1:1 glycerol/mineral oil and the amount of cell-associated penton base was determined by counting the cell pellet in a  $\gamma$  counter.

The effect of the DAV-1 mAb on adenovirus infection was quantified by plaque assay. A549 cells were seeded into six-well plates and cultured to 90% confluency. Three  $\mu$ g/ml of DAV-1 Fab or 18  $\mu$ g of whole IgG DAV-1 antibody were added to the cell cultures, followed by addition of purified 100 p.f.u. Ad2 and incubation at 37°C for 2 h. The Ad2 and antibody mixtures were then removed, and 8 ml of overlay medium containing 0.5% agarose in DMEM medium and 10% FCS was added into each well. The cells were fed with 4 ml of overlay medium on day 5 post-infection. The plaques were scored on day 10 post-infection.

### **Epitope mapping and kinetic analysis of DAV-1 binding to penton base**

The DAV-1 binding site on the Ad2 penton base was identified by affinity-directed mass spectrometry (Zhao and Chait, 1994; Zhao *et al.*, 1996). For these studies, we arbitrarily selected a region of the penton base that approximately spanned the RGD sequence. A series of overlapping synthetic peptides varying by one amino acid on the N-terminal or C-terminal region of the Ad2 penton base RGD sequence, <sup>480</sup>MNDHAIARGDTFATRA<sup>494</sup>, was generated by solid-phase protocols (Zhao and Chait, 1994; Zhao *et al.*, 1996). The precise boundaries of

the DAV-1 epitope were then determined by affinity-directed mass spectrometry as described previously (Zhao and Chait, 1994; Zhao *et al.*, 1996).

Precise measurements of DAV-1 interactions with the penton base protein were determined by SPR (Karlsson *et al.*, 1991) using an automated biosensor system (BIAcore 2000 Pharmacia). Briefly, recombinant penton base at 60 µg/ml was immobilized onto carboxymethyl dextran-coated biosensor chips in 10 mM MES pH 6.5 containing 10 mM NaCl. Following amine coupling of the penton base, varying amounts of purified Fab fragments (3.6–57.0 µg/ml) or IgG molecules (36–576 µg/ml) were flowed over the penton base at a rate of 40 µl or 5 µl/min, respectively. Kinetic binding data ( $K_{on}$ ,  $K_{off}$  and  $K_D$ ) were obtained using BIAevaluation software (version 2.1). Stoichiometric data was obtained by observing the change in SPR at saturation binding and assuming a molecular mass of 350 kDa for the penton base, 43 kDa for Fab fragments and 150 kDa for IgG molecules.

### Cryo-EM

The final volume of the virus preparation was adjusted to achieve a virus concentration of  $\sim 8 \times 10^{11}$  particles/ml which we have found to be optimal for well-spaced particles on the cryo-grid. An excess of concentrated Fab was added to adenovirus in a Fab:binding site ratio of 15:1.  $Ca^{2+}$  and  $Mg^{2+}$  ions were added to the mixture to stabilize the resultant complexes. The mixture was allowed to incubate for 1 h on ice (0°C) before applying the samples to cryo-grids.

Cryo-grids of the adenovirus–Fab complex and a separate sample of uncomplexed adenovirus were prepared according to well-established procedures (Adrian *et al.*, 1984). A 4 µl droplet of concentrated sample was applied to a glow-discharged holey carbon grid. The grid was briefly blotted with filter paper and plunged into ethane slush chilled by liquid nitrogen. The rapid cooling produces vitreous (amorphous), rather than crystalline, ice. The frozen grid was then transferred to liquid nitrogen, placed in a pre-chilled Gatan 626 cryo-transfer holder, and inserted into a Philips CM120 transmission electron microscope. Images were collected with a Gatan slow-scan CCD camera under low dose conditions ( $< 20$  electrons/Å<sup>2</sup>) at a nominal magnification of 45 000× and 1.5 µm underfocus. The pixel size of the digital images was calibrated with a catalase crystal and found to be 4.1 Å.

### Image processing

Individual adenovirus particles in random orientations were extracted as 274×274 pixel fields from the digital micrographs (1024×1024 pixels). A circular mask was applied and the particles were background subtracted using CRIISP, an in-house IDL-based (Research Systems, Inc.) image processing package. The IMAGIC software package (van Heel and Keegstra, 1981; van Heel *et al.*, 1996) was used to normalize the means and variances of the images, translationally align the images to a generated reference (the rotationally averaged sum of the input images), and determine the icosahedral view angles via the technique of angular reconstitution (van Heel, 1987). The angles were refined and checked for hand agreement with the SIMPLEX program from the icosahedral image reconstruction suite (Fuller *et al.*, 1996). A preliminary three-dimensional reconstruction was generated with IMAGIC by exact filtered back projection methods (Hamming filter factor = 0.75). IMAGIC imposes icosahedral symmetry by using all particle images 60 times during the reconstruction process (M.van Heel, in preparation). The exact filter reconstruction technique corrects for the uneven distribution of particle orientations within the asymmetric triangle (Harauz and van Heel, 1986). Further translational refinement of the input images was carried out by projecting the reconstruction in the view angles of the input images and then translating the input images to maximize the cross-correlation coefficient with their corresponding projections.

A final reconstruction of 128<sup>3</sup> voxels (at 8.7 Å per edge of voxel) was calculated by exact filtered back projection for both the adenovirus–Fab complex and the uncomplexed adenovirus particle. To calculate the difference between these two maps, only voxels in the adenovirus reconstruction with density values above the mean were subtracted from the adenovirus–Fab map. This resulted in a clean subtraction of the capsid density, including the penton base protrusions, from the adenovirus–Fab reconstruction. The resolution of the reconstructions was evaluated by the IMAGIC Fourier ring correlation function using a 2σ cutoff. An additional resolution test was carried out by comparing the shape of the hexon protein in the reconstruction with the crystallographic hexon filtered to 14, 19 and 24 Å resolution using a Fermi filter. The hexon filtered to 19 Å resolution showed the best qualitative agreement with the features in the reconstruction. The three-dimensional reconstructions were viewed with AVS (Advanced Visualization Systems, Inc.), on a

Unix-based Digital Equipment Corp. (DEC) Alpha 3000 workstation equipped with a Kubota (Kubota Graphics Corp.) five-processor high-speed graphics accelerator board. Correction for the CTF of the electron microscope was carried out using an AVS deconvolution module (Stewart *et al.*, 1993). The parameters used for the CTF equation ( $C_s = 2$  mm for a Philips CM120 electron microscope, fraction of amplitude contrast = 0.1, defocus =  $-1.5$  µm,  $kV = 120$ , decay constant = 20 nm<sup>2</sup>, Fermi filter resolution cutoff = 19 Å, filter width = 5 Å) were selected to equalize background density and minimize defocus ‘ringing’ effects as observed in the central slice of the reconstruction.

Volume measurements were performed as in Stewart *et al.* (1993) by summing the number of voxels above a specified contour level. The appropriate level was chosen as the point where the volume of the capsid changed the least with a fixed change in contour level. This value was used as the isosurface level for the figures of the adenovirus capsid and penton base protein. To visualize and measure the volume of the weak penton base protrusion and the Fab density, the isosurface level was lowered to the mean density value of the reconstruction which was just above the noise level in the map. The integrated Fab density in the deconvolved reconstruction was calculated by summing all of the voxel density values within the volume defined by the isosurface just above the noise level. The expected Fab density and volume were determined by comparison with measurements on the penton base protein.

### Fab coordinate modeling

The crystallographic coordinates of a Fab fragment from a mAb directed against FMDV (Verdaguer *et al.*, 1995) were mapped into the cryo-EM Fab density. Eight copies of the Fab coordinates were positioned in distinct orientations in order to span completely the observed cryo-EM Fab density. Tilt angles for the modeled Fab fragments were determined by measuring the solid angle between the pseudo-dyad Fab axis and the fiber axis. Rough density maps were calculated from the modeled Fab coordinates by summing the atomic masses of all the non-hydrogen atoms within voxels of the same size as in the cryo-EM reconstruction. The density maps were then filtered to 19 Å, the resolution of the cryo-EM reconstruction, using a Fermi filter.

## Acknowledgements

The authors thank Dr Ignasi Fita at the Universitat Politècnica de Catalunya in Barcelona for providing the Fab/RGD peptide coordinates and Dr Ron Milligan at The Scripps Research Institute for generously allowing use of his electron microscope during the initial stages of the project. The authors also express their gratitude to Bonnie Bradt and Dwayne Stupack for initial studies on the production and analyses of the DAV-1 mAb; to Mithra Mahmoudi, Katie McGuire, Mark Sakaguchi and James Masse for initial image processing; and to Pranab Banerjee for customizing the CRIISP image processing package. We also thank Steve Fuller for supplying the latest UNIX versions of the icosahedral programs and Tim Baker and Tom Smith for helpful discussions. This work was supported with NIH grant HL54352 to G.R.N. and a UCLA School of Medicine Frontiers of Science grant to P.L.S. C.Y.C. is supported by a fellowship from the Life and Health Medical Insurance Research Fund. This is manuscript No. 9195-IMM at The Scripps Research Institute, La Jolla, CA.

## References

- Acharya, R., Fry, E., Stuart, D., Fox, G., Rowlands, D. and Brown, F. (1989) The three-dimensional structure of foot-and-mouth disease virus at 2.9 Å resolution. *Nature*, **337**, 709–716.
- Adler, M., Lazarus, R.A., Dennis, M.S. and Wagner, G. (1991) Solution structure of Kistrin, a potent platelet aggregation inhibitor and GP IIb-IIIa antagonist. *Science*, **253**, 445–448.
- Adrian, M., Dubochet, J., Lepault, J. and McDowell, A.M. (1984) Cryo-electron microscopy of viruses. *Nature*, **308**, 32–36.
- Athappilly, F.K., Murali, R., Rux, J.J., Cai, Z. and Burnett, R.M. (1994) The refined crystal structure of hexon, the major coat protein of adenovirus type 2, at 2.9 Å resolution. *J. Mol. Biol.*, **242**, 430–455.
- Atkinson, R.A., Saudek, V. and Pelton, J.T. (1994) Echistatin: the refined structure of a disintegrin in solution by <sup>1</sup>H NMR and restrained molecular dynamics. *Int. J. Peptide Protein Res.*, **43**, 563–572.
- Bai, M., Harfe, B. and Freimuth, P. (1993) Mutations that alter an Arg-Gly-Asp (RGD) sequence in the adenovirus type 2 penton base protein abolish its cell-rounding activity and delay virus reproduction in flat cells. *J. Virol.*, **67**, 5198–5205.

- Berinstein, A., Roivainen, M., Hovi, T., Mason, P.W. and Baxt, B. (1995) Antibodies to the vitronectin receptor (integrin  $\alpha v \beta_3$ ) inhibit binding and infection of foot-and-mouth disease virus to cultured cells. *J. Virol.*, **69**, 2664–2666.
- Brandt, C.D., Kim, H.W., Vargosko, A.J., Jeffries, B.C., Arrobio, J.O., Rindge, B., Parrott, R.H. and Chanock, R.M. (1969) Infections in 18,000 infants and children in a controlled study of respiratory tract disease: Adenovirus pathogenicity in relation to serologic type and illness syndrome. *Am. J. Epidemiol.*, **90**, 484–500.
- Brody, S.L. and Crystal, R.G. (1994) Adenovirus-mediated *in vivo* gene therapy. *Ann. NY Acad. Sci.*, **716**, 90–103.
- Dales, S. and Chardonnet, Y. (1973) Early events in the interaction of adenoviruses with HeLa cells: Association with microtubules and the nuclear pore complex during vectorial movement of the inoculum. *Virology*, **56**, 465–483.
- Defer, C., Belin, M.-T., Caillet-Boudin, M.-L. and Boulanger, P. (1990) Human adenovirus-host cell interactions: comparative study with members of subgroups B and C. *J. Virol.*, **64**, 3661–3673.
- Everitt, E., Meador, S.A. and Levine, A.S. (1977) Synthesis and processing of the precursor to the major core protein of adenovirus type 2. *J. Virol.*, **21**, 199–214.
- Fitzgerald, D.J.P., Padmanabhan, R., Pastan, I. and Willingham, M.C. (1983) Adenovirus-induced release of epidermal growth factor and pseudomonas toxin into the cytosol of KB cells during receptor-mediated endocytosis. *Cell*, **32**, 607–617.
- Fuller, S.D., Butcher, S.J., Cheng, R.H. and Baker, T.S. (1996) Three-dimensional reconstruction of icosahedral particles - the uncommon line. *J. Struct. Biol.*, **116**, 48–55.
- Goldman, M.J. and Wilson, J.M. (1995) Expression of  $\alpha v \beta 5$  integrin is necessary for efficient adenovirus-mediated gene transfer in the human airway. *J. Virol.*, **69**, 5951–5958.
- Greber, U.F., Willetts, M., Webster, P. and Helenius, A. (1993) Stepwise dismantling of adenovirus 2 during entry into cells. *Cell*, **75**, 477–486.
- Greber, U.F., Webster, P., Helenius, A. and Weber, J. (1996) The role of the adenovirus protease in virus entry into cells. *EMBO J.*, **15**, 1766–1777.
- Harauz, G. and van Heel, M. (1986) Exact filters for general geometry three dimensional reconstruction. *Optik*, **73**, 146–156.
- Hewat, E.A. and Blaas, D. (1996) Structure of a neutralizing antibody bound bivalently to human rhinovirus 2. *EMBO J.*, **15**, 1515–1523.
- Horwitz, M.S. (1990) Adenoviridae and their replication. In Fields, B.N. and Knipe, D.M. (eds), *Virology*. Raven Press, New York, pp. 1679–1721.
- Huang, S., Endo, R.I. and Nemerow, G.R. (1995) Upregulation of integrins  $\alpha v \beta 3$  and  $\alpha v \beta 5$  on human monocytes and T lymphocytes facilitates adenovirus-mediated gene delivery. *J. Virol.*, **69**, 2257–2263.
- Karlsson, R., Michaelsson, A. and Mattsson, L. (1991) Kinetic analysis of monoclonal antibody-antigen interactions with a new biosensor based analytical system. *J. Immunol. Methods*, **145**, 229–240.
- Lea, S., Hernandez, J., Blakemore, W., Brocchi, E., Curry, S., Domingo, E., Fry, E., Abu-Ghazaleh, R., King, A., Newman, J. and Mateu, M.G. (1994) The structure and antigenicity of a type C foot-and mouth disease virus. *Structure*, **2**, 123–139.
- Liu, H., Smith, T.J., Lee, W., Mosser, A.G., Rueckert, R.R., Olson, N.H., Cheng, R.H. and Baker, T.S. (1994) Structure determination of an Fab fragment that neutralizes human rhinovirus 14 and analysis of the Fab-virus complex. *J. Mol. Biol.*, **240**, 127–137.
- Main, A.L., Harvey, T.S., Baron, M., Boyd, J. and Campbell, I.D. (1992) The three-dimensional structure of the tenth type III module of fibronectin: An insight into RGD-mediated interactions. *Cell*, **71**, 671–678.
- Mathias, P., Wickham, T.J., Moore, M. and Nemerow, G. (1994) Multiple adenovirus serotypes use  $\alpha v$  integrins for infection. *J. Virol.*, **68**, 6811–6814.
- Nemerow, G.R., Wickham, T.J. and Cheresch, D.A. (1993) The role of  $\alpha v$  integrins in adenovirus infection. In Preissner, K.T., Rosenblatt, S., Kost, C., Wegerhoff, J. and Mosher, D.F. (eds), *Biology of Vitronectins and Their Receptors*. Elsevier Science, Amsterdam, The Netherlands, pp. 177–184.
- Neumann, R., Chroboczek, J. and Jacrot, B. (1988) Determination of the nucleotide sequence for the penton-base gene of human adenovirus type 5. *Gene*, **69**, 153–157.
- Parry, N., Fox, G., Rowlands, D., Brown, F., Fry, E., Acharya, R., Logan, D. and Stuart, D. (1990) Structural and serological evidence for a novel mechanism of antigenic variation in foot-and-mouth disease virus. *Nature*, **347**, 569–572.
- Porta, C., Wang, G., Cheng, H., Chen, Z., Baker, T.S. and Johnson, J.E. (1994) Direct imaging of interactions between an icosahedral virus and conjugate  $F_{ab}$  fragments by cryoelectron microscopy and X-ray crystallography. *Virology*, **204**, 777–788.
- Seth, P., Fitzgerald, D., Ginsberg, H., Willingham, M. and Pastan, I. (1984) Evidence that the penton base of adenovirus is involved in potentiation of toxicity of *Pseudomonas* exotoxin conjugated to epidermal growth factor. *Mol. Cell Biol.*, **4**, 1528–1533.
- Seth, P., Willingham, M.C. and Pastan, I. (1985) Binding of adenovirus and its external proteins to triton X-114. *J. Biol. Chem.*, **260**, 14431–14434.
- Smith, T.J., Chase, E.S., Schmidt, T.J., Olson, N.H. and Baker, T.S. (1996) Neutralizing antibody to human rhinovirus 14 penetrates the receptor-binding canyon. *Nature*, **383**, 350–354.
- Smith, T.J., Olson, N.H., Cheng, R.H., Liu, H., Chase, E.S., Lee, W.M., Leippe, D.M., Mosser, A.G., Rueckert, R.R. and Baker, T.S. (1993) Structure of human rhinovirus complexed with Fab fragments from a neutralizing antibody. *J. Virol.*, **67**, 1148–1158.
- Smith, T.J., Cheng, R.H., Olson, N.H., Peterson, P., Chase, E., Kuhn, R.J. and Baker, T.S. (1995) Putative receptor binding sites on alphaviruses as visualized by cryoelectron microscopy. *Proc. Natl Acad. Sci. USA*, **92**, 10648–10652.
- Stewart, P.L., Burnett, R.M., Cyrklaff, M. and Fuller, S.D. (1991) Image reconstruction reveals the complex molecular organization of adenovirus. *Cell*, **67**, 145–154.
- Stewart, P.L., Fuller, S.D. and Burnett, R.M. (1993) Difference imaging of adenovirus: Bridging the resolution gap between X-ray crystallography and electron microscopy. *EMBO J.*, **12**, 2589–2599.
- Svensson, U. (1985) Role of vesicles during adenovirus 2 internalization into HeLa cells. *J. Virol.*, **55**, 442–449.
- van Heel, M. (1987) Angular reconstitution: A posteriori assignment of projection directions for 3D reconstruction. *Ultramicroscopy*, **21**, 111–124.
- van Heel, M. and Keegstra, W. (1981) IMAGIC: A fast, flexible and friendly image analysis software system. *Ultramicroscopy*, **7**, 113–130.
- van Heel, M., Harauz, G., Orlova, E.V., Schmidt, R. and Schatz, M. (1996) A new generation of the IMAGIC image processing system. *J. Struct. Biol.*, **116**, 17–24.
- Verdaguer, N., Mateu, M.G., Andreu, D., Giralt, E., Domingo, E. and Fita, I. (1995) Structure of the major antigenic loop of foot-and-mouth disease virus complexed with a neutralizing antibody: direct involvement of the Arg-Gly-Asp motif in the interaction. *EMBO J.*, **14**, 1690–1696.
- Wadell, G., Allard, A., Johansson, M., Svensson, L. and Uhnoo, I. (1987) Enteric adenoviruses. *Ciba Found. Symp.*, **128**, 63–91.
- Wickham, T.J., Mathias, P., Cheresch, D.A. and Nemerow, G.R. (1993) Integrins  $\alpha v \beta 3$  and  $\alpha v \beta 5$  promote adenovirus internalization but not virus attachment. *Cell*, **73**, 309–319.
- Wickham, T.J., Filardo, E.J., Cheresch, D.A. and Nemerow, G.R. (1994) Integrin  $\alpha v \beta 5$  selectively promotes adenovirus mediated cell membrane permeabilization. *J. Cell Biol.*, **127**, 257–264.
- Zhao, Y. and Chait, B.T. (1994) Protein epitope mapping by mass spectrometry. *Anal. Chem.*, **66**, 3723–3726.
- Zhao, Y., Muir, T.W., Kent, S.B.H., Tischer, E., Scardina, J.M. and Chait, B.T. (1996) Mapping protein-protein interactions by affinity-directed mass spectrometry. *Proc. Natl Acad. Sci. USA*, **93**, 4020–4024.

Received on August 30, 1996; revised on November 15, 1996

## Note added in proof

The penton base of Ad3 was recently shown to also have a flexible surface loop [Schoen et al. (1997) *EMBO J.*, **15**, 6841–6846].